Arabian Journal of Chemistry (2022) **15**, 103753

King Saud University

Arabian Journal of Chemistry

www.ksu.edu.sa
www.sciencedirect.com

ORIGINAL ARTICLE

Zinc oxide nanoparticles promotes ferroptosis to repress cancer cell survival and inhibits invasion and migration by targeting miR-27a-3p/YAP axis in renal cell carcinoma

Xingyuan Wang [a], Dechao Li [a], Zhinan Xia [b], Lichen Teng [a], Yongsheng Chen [a], Jie Meng [c], Changfu Li [a,*]

[a] *Department of Urology, Harbin Medical University Cancer Hospital, Harbin, Heilongjiang Province, China*
[b] *Department of Urology, The First Affiliated Hospital of Harbin Medical University, Harbin, Heilongjiang Province, China*
[c] *Department of Maxillofacial Cosmetic Surgery, Heilongjiang Provincial Hospital, Harbin, Heilongjiang Province, China*

Received 13 December 2021; accepted 29 January 2022
Available online 3 February 2022

KEYWORDS

RCC;
Ferroptosis;
ZONs;
miR-27a-3p;
YAP

Abstract *Background:* Renal cell carcinoma (RCC) is a prevalent malignancy with growing mortality and high metastasis. Ferroptosis has been identified as an essential process in cancer development, but the regulatory mechanism underlying the RCC progression remains obscure. The nanomaterial zinc oxide nanoparticles (ZONs) have presented anti-cancer function. Here, we identified the critical role of ZONs in promoting ferroptosis of RCC cells by regulating miR-27a-3p/YAP axis.

Methods: The effect of ZONs on RCC was analyzed by qPCR, Western blot, MTT assays, colony formation assays, Flow cytometry analysis, transwell assays, wound healing assays, iron assays, lipid ROS detection, luciferase reporter gene assays, and tumor xenograft.

Results: The treatment of ZONs repressed expression of GPX4 and SLC7A11 and enhanced ROS accumulation and iron/Fe^{2+} levels in RCC cells. Ferroptosis activator erastin repressed RCC cell viabilities and ZONs further repressed this effect. ZONs inhibited invasion and migration of RCC cells and treatment of ZONs represses RCC cell survival *in vitro*. ZONs suppressed RCC cell growth in tumorigenicity mouse model. Mechanically, ZONs down-regulated YAP expression by inducing miR-27a-3p, in which YAP overexpression and miR-27a-3p inhibition reverse ZONs -inhibited RCC cell survival *in vitro*.

* Corresponding author.at: Department of Urology, Harbin Medical University Cancer Hospital, Harbin, Heilongjiang Province, China.
E-mail address: changfauldh05044@163.com (C. Li).

Peer review under responsibility of King Saud University.

Production and hosting by Elsevier

https://doi.org/10.1016/j.arabjc.2022.103753

Discussion: Thus, we concluded that ZONs induced RCC cell ferroptosis to suppress RCC cell survival by targeting miR-27a-3p/YAP axis. The clinical significance of ZONs for the treatment of RCC is required to further study and may benefit the targeted therapy of RCC.

1. Background

Renal cell carcinoma (RCC) is a leading cause of cancer-related death globally (Linehan and Ricketts, 2019). Despite the development of therapeutic methods, the prognosis of RCC remains unsatisfactory (Lucarelli et al., 2019). Hence, its urgent to develop novel therapeutic targets. Ferroptosis is a novel form of regulated cell death driven by iron-dependent lipid peroxidation, which differs from other types of cell death including apoptosis, necrosis, and autophagy, in the aspects of morphology, genetics and biochemistry (Dixon et al., 2012). During the process of ferroptosis, increased free iron and accumulated lipid peroxides are regarded as two main participants, which lead to increased intracellular reactive oxygen species (Miess et al., 2018) production and subsequent oxidative cell death (Yagoda et al., 2007). Recent studies are gradually revealing the role of ferroptosis during RCC development and its potential as a novel therapeutic target for RCC treatment. For example, the Hippo signaling regulator TAZ modulates ferroptosis in RCC (Yang et al., 2019). These studies suggested the potential role of ferroptosis as a target for lung cancer therapy. Moreover, Zinc oxide nanoparticles (ZONs) are the nanomaterial that have been applied in industrial products and are capable of targeting multiple cancer cell types and cancer stem cells (Steele et al., 2009; Hu and Du, 2020). However, the effect of ZONs on ferroptosis of RCC cells is still unclear.

Yes-associated protein (YAP) is one of the primary effectors of the Hippo pathway, functions as a transcriptional regulator to facilitate expression of pro-growth genes and suppress apoptotic genes (Maugeri-Sacca and De Maria, 2018). A recent study indicated that miR-27a directly target YAP1, as well as downregulating the levels of Twist and Snail to notably decrease the invasiveness of oral squamous cell carcinoma cells (Zeng et al., 2016). Moreover, Jiang et al. found that Merlin-HIPPO-YAP signaling is associated with ferroptosis susceptibility of metastasis-prone epithelial cells, suggesting the potential association between YAP and ferroptosis (Wu et al., 2019).

In this study, we aimed to determine the role of ZONs in RCC, and the related mechanisms. Here, we found ZONs repressed RCC growth and metastasis by inducing ferroptosis, and deciphered the mechanisms involving its effect on miR-27a-3p and subsequent release of YAP protein. Ultimately, our work provided a promising therapeutic strategy promoting ferroptosis through ZONs/miR-27a-3p/YAP regulatory axis in RCC.

2. Materials and methods

2.1. Cell culture and transfection

Human RCC cell lines (786-O, 769P and CAKI-1) were purchased from the American Type Culture Collection (ATCC, USA), and cultured with Dulbecco's modified Eagle's medium (DMEM, Gibco, CA, USA) containing 10% FBS (Gibco), 1% penicillin and streptomycin (Sigma, USA), in a 37 °C humidified incubator with 5% CO_2. The YAP overexpression plasmid, miR-27-3p mimics and the negative controls were designed by and purchased from RiboBio (Shanghai, China). The cell transfection was conducted by using Lipofectamine 3000 (Life Technologies, CA, USA) following manufactures' instruction. For *in vitro* study, cells were treated with Erastin (5 μM), and/or ZONs (30 μg/mL) for 24 h.

2.2. Patients and tissue samples

We included 50 RCC patients, who received surgical operation in our hospital, in a clinical follow-up study for nine years. Tumor tissues were collected during operation and subjected to real-time PCR to evaluate the level of miR-27-3p, and YAP. All experiments have acquired the consents of patients and were performed under approval of Harbin Medical University Cancer Hospital. And were carried out in compliance with the ethical standards of the Declaration of Helsinki.

2.3. RNA extraction and quantification

The total RNA of RCC cells was extracted using a TRIzol reagent (Invitrogen, CA, USA), reversely transcribed to cDNA using a SuperScript®VILO™ cDNA synthesis kit (Invitrogen). Quantification of the cDNA was performed by real-time qPCR using a Fast SYBR™ Green Master Mix kit (Thermo, MA, USA). GAPDH and U6 were used as internal control for normalization of mRNA and the noncoding RNAs. The relative change in RNA levels were calculated by $2^{-\Delta\Delta Ct}$ method. The primer sequences were as follows: miR-27-3p: sense, 5′-GAACTTAGCCACTGTGAACACCACTTGG-3′, antisense, 5′-TTGCTTCCTGTCACAAATCACATTG-3′; U6: sense, 5′-AAAGCAAATCATCGGACGACC-3′, antisense, 5′-GTACAACACATTGTTTCCTCGGA-3′.

2.4. Cell viability assay

The cell viability was detected by MTT assay. The cells were conducted with indicated treatment, and placed in 96-well plates at a density of 4×10^3 cells per well to growth for 48 h. Then 10 μL (5 mg/mL) of MTT reagent was added in each well to incubate for another 4 h. At the end time point, the medium with MTT were discarded and 150 μL DMSO were added in each well. The absorbance values were detected at 490 nm using a microplate reader (PerkinElmer, CA, USA).

2.5. Colony formation

The cells were conducted with indicated treatment, and placed in 6-well plates at a density of 500 cells per well, and maintained in

normal culture condition to allow formation of mono colonies. After incubation for 12 days, the colonies were fixed and stained by 0.5% crystal violet in methanol for 30 min. The colonies were captured under a microscope (Olympus, Japan) and counted.

2.6. Flow cytometry of apoptosis

The intrinsically induced apoptotic cell death was detected by flow cytometry analysis. The cells were seeded in 6-well plate at a density of 5×10^5/well and conducted with indicated treatment for 48 h. Next, the cells were digested with EDTA-free trypsin to single-cell and collected, followed by re-suspension in binding buffer and incubation with PI and Annexin-FITC at room temperature for 15 min in dark. Then the suspension was detected in a Flow cytometry (BD bioscience) to collect fluorescence signals.

2.7. Transwell assay

Cell invasion ability was detected by transwell experiment using Transwell chambers (Corning, CA, USA). Cells were pretreated as indicated, and seed in upper chambers containing FBS-free medium at a density of 2×10^4/well, whereas the bottom chamber were added with DMEM medium containing 10% FBS. After incubation for 48 h, the upper chambers were fixed and stained with 0.5% crystal violet in methanol for 30 min, captured and counted. For cell invasion experiment, the chambers were pre-coated with Matrigel (Corning).

2.8. Wound healing assay

Cells were transfected with indicated RNAs and seeded in 6-well plate at a density of 5×10^5/well to form a monoplayer. A sterilized 200 ul pipette were used to gently scratch a line on the monoplayer. Then the cells were washed with PBS to wash out the detached cells, and replaced with fresh FBS-free medium for continuing incubation. The images of scratch were captured at 0 h, 6 h and 12 h after scratching with a microscope (Olympus), and measured.

2.9. Iron assay

The intracellular Fe^{2+} level was determined by an iron assay kit (Beyotime, Shanghai, China) following the manufacturer's instruction. Briefly, cells were seeded in 6-well plate at a density of 5×10^5/well, collected and homogenized. Next, the supernatant was mixed with iron probe after incubation with iron reducer. The absorbance values at 590 nm were measured by a microplate reader (PerkinElmer).

2.10. Lipid ROS detection

The lipid ROS level of cells was determined by BODIPY C-11 staining (Beyotime, Shanghai, China). Cells were seeded in 6-well plate at a density of 5×10^5/well, stained with BODIPY C-11 dye for 30 min. Subsequently, the cells were collected and detected by Flow cytometry (BD bioscience).

2.11. Western blotting

The cells were lysed by RIPA lysis buffer to collected total proteins. Then the protein samples were separated by SDS-PAGE and transferred to a PVDF membrane, followed by blocking with 5% nonfat milk. The blots were incubated with specific primary antibodies, which refer to anti-GPX4 (1:1000), SLC7A11 (1:1000), anti-YAP (1:1000), anti-Snail (1:1000), anti-Twist (1:1000), anti-E-cadherin (1:1000) , anti-Vimentin (1:1000), and anti-β-actin (1:2000), at 4℃ overnight. Next day, the blots were incubated with corresponding secondary antibodies for 2 h at room temperature. The visualization of blots was performed by using a ECL kit (Invitrogen), and captured by an imaging system (BD). All antibodies were purchased from Abcam (MA, USA).

2.12. Luciferase reporter gene assay

The potential binding sites between miR-27a-3p with 3′UTR of YAP were predicted by online website ENCORI and TargetScan. The wide type and mutated sequence of 3′UTR of YAP (YAP-WT and YAP-Mut) were inserted into psi-CHECK2 plasmid (Promega, WI, USA). The cells were seeded in 12-well plate at a density of 2×10^5/well, followed by co-transfection with indicated luciferase reporter plasmids and miR-27a-3p mimics or the negative control (NC) for 48 h. Then the cells were collected and lysed, and the luciferase activity was measured by the dual-luciferase reporter assay system (Promega, WI, USA) following the manufacture's instruction.

2.13. Tumor xenograft

Ten SCID/nude mice aged 6–8 weeks were purchased from Vital River (Beijing, China), and randomly divided into two groups. Subsequently, CAKI-1 cells were suspended in saline at a density of 5×10^6/100 μL, and were subcutaneously injected to left back of each mouse. Tumor volume ($V = \text{length} \times \text{width}^2/2$) and mice body weight were measured every 3 days. Thirty days later, the mice were succumbed to death and the tumors were isolated for following experiments. All procedures performed in studies involving animals were in accordance with the ethical standards of the Harbin Medical University Cancer Hospital at which the studies were conducted.

2.14. Statistics

All data in this study were presented as mean ± standard deviation (SD), and were analyzed by SPSS25.0 software. Statistic comparison between two groups or multiple groups were evaluated by Student's *t* test or one-way ANOVA. P value < 0.05 were set as threshold for statistically significant.

3. Results

3.1. ZONs induce ferroptosis-like phenotypes in RCC cells

Interestingly, we observed that the treatment of ZONs repressed expression of ferroptosis-negative regulated factors,

including GPX4 and SLC7A11 in CAKI-1, 786-O, and 769P cells (Fig. 1A and S1A). The ferroptosis related phenotypes, such as ROS accumulation and iron/Fe^{2+} levels, were enhanced by ZONs in CAKI-1, 786-O, and 769P cells (Fig. 1-B-D and S1B-D). Ferroptosis activator erastin repressed CAKI-1, 786-O, and 769P cell viabilities and ZONs promoted this effect (Fig. 1E and Fig. S1E).

3.2. ZONs reduce invasion and migration of RCC cells

Next, we were interested in the correlation of ZONs with RCC cell invasion and migration *in vitro*. Wound healing assays showed that ZONs enhanced wound proportion in CAKI-1, 786-O, and 769P cells and indicated that ZONs inhibited CAKI-1, 786-O, and 769P cell migration (Fig. 2A and B, and Fig. S2A). Meanwhile, ZONs attenuated the migrated and invaded abilities of CAKI-1, 786-O, and 769P cells (Fig. 2C and D, and Fig. S2B). Meanwhile, the treatment of ZONs repressed expression of Twist, and Vimentin and enhanced E-cadherin expression (Fig. 2E, and Fig. S2C).

3.3. ZONs repress RCC cell survival in vitro

Furthermore, our data revealed that ZONs reduced CAKI-1, 786-O, and 769P cell viabilities (Fig. 3A and S3A). More obviously, the colony numbers of CAKI-1, 786-O, and 769P cells were decreased by ZONs in the colony formation assays (Fig. 3B and C, and S3B). ZONs significantly induced CAKI-1, 786-O, and 769P cell apoptosis (Fig. 3D and E, and Fig. S3C).

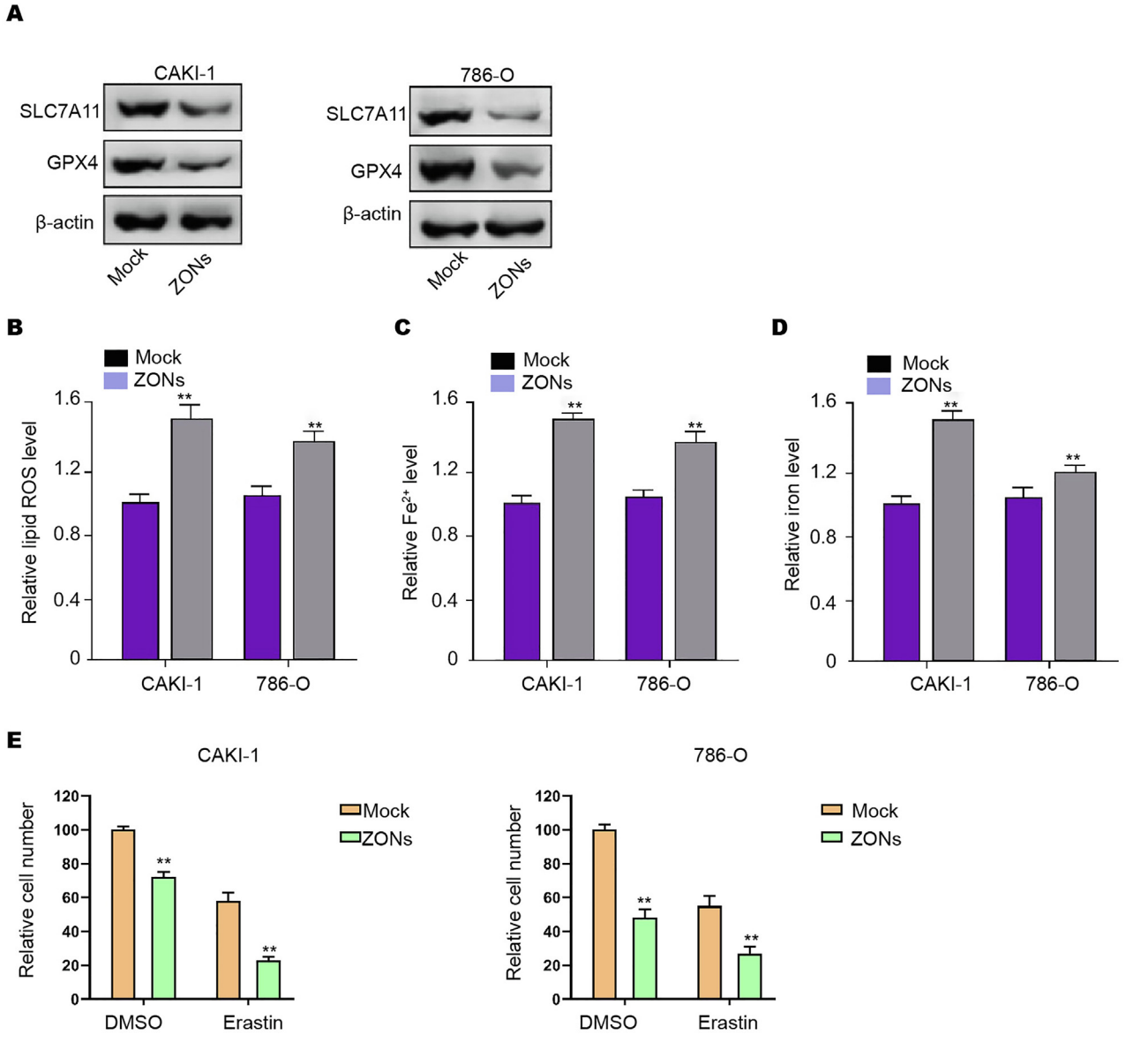

Fig. 1 ZONs induce ferroptosis-like phenotypes in RCC cells. (A) Western blot analysis of GPX4 and SLC7A11 (B), ROS analysis (C), iron/Fe^{2+} analysis (D) were conducted in CAKI-1 and 786-O cells treated with ZONs. (E) MTT assays were performed in the CAKI-1 and 786-O cells treated as the indicated labeling. N = 3, mean ± SD: ** $P < 0.01$.

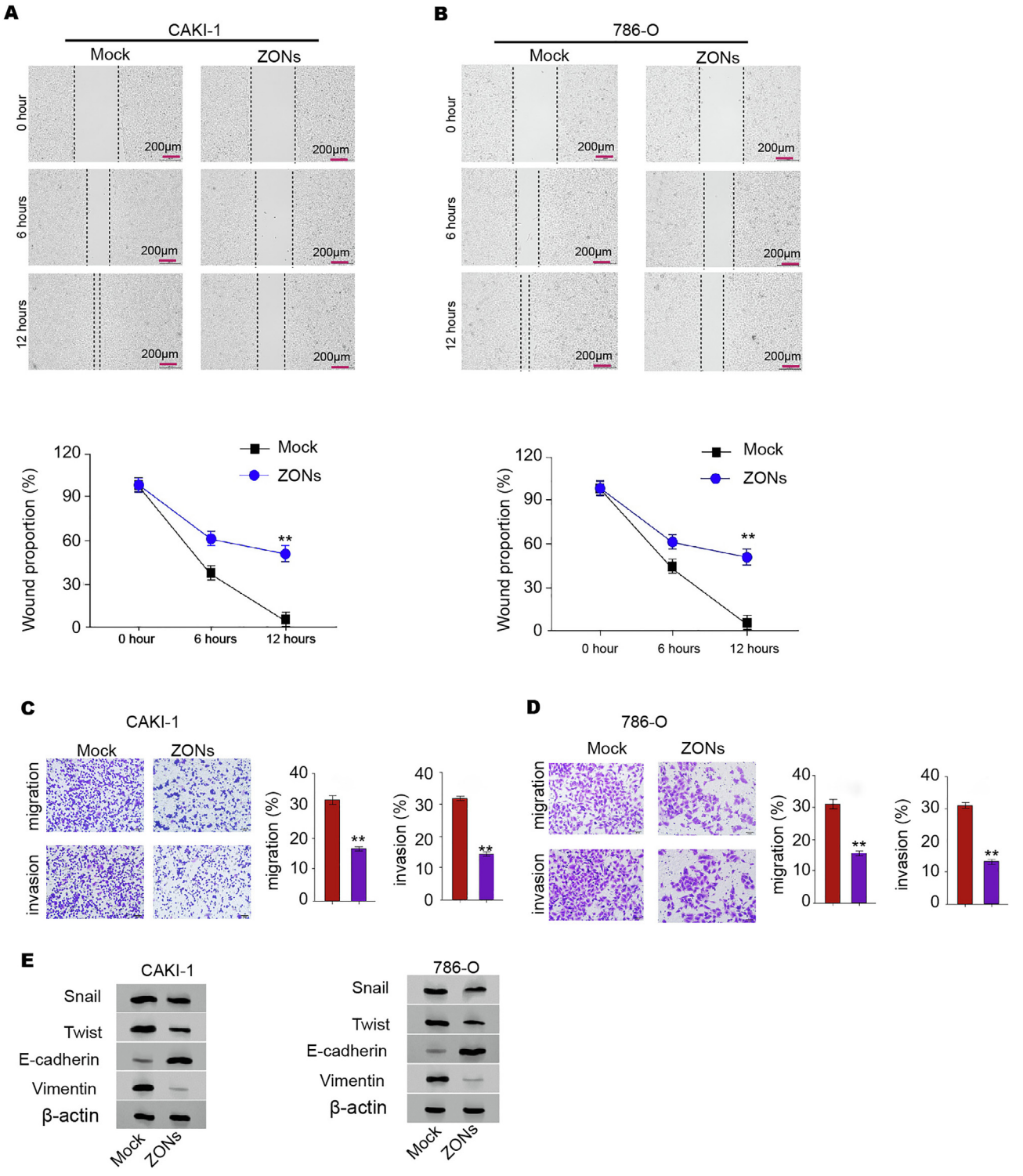

Fig. 2 ZONs reduce invasion and migration of RCC cells. (A-E) The wound healing assays (A and B) and transwell assays (C and D) were performed in CAKI-1 and 786-Ocells treated with ZONs. (E) The expression of Snail, Twist, Vimentin, and E-cadherin was analyzed by Western blot. N = 3, mean ± SD: ** $P < 0.01$.

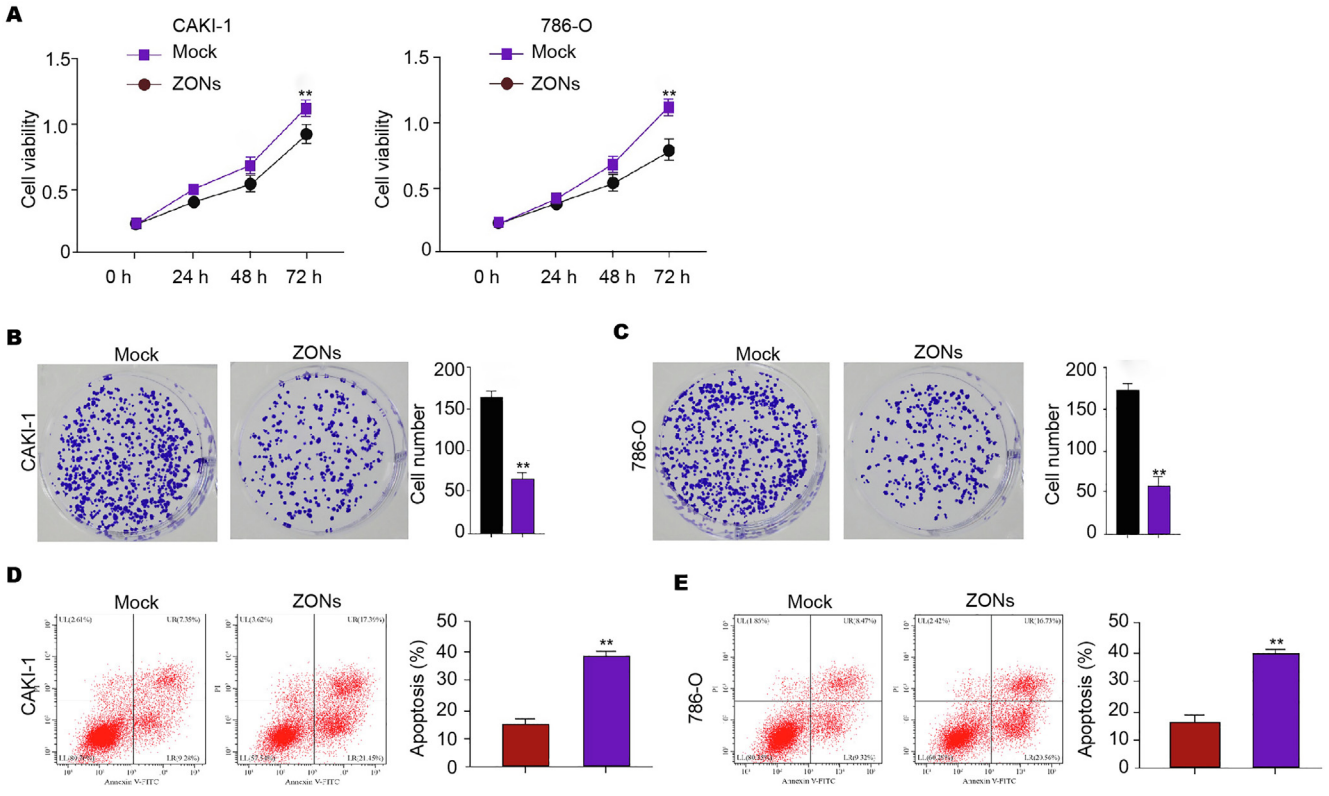

Fig. 3 ZONs repress RCC cell survival *in vitro*. (A-E) The MTT assays (A), colony formation analysis (B and C), Flow cytometry analysis of apoptosis (D and E) were carried out in the CAKI-1 and 786-O cells treated with ZONs. N = 3, mean ± SD: ** $P < 0.01$.

3.4. ZONs suppress RCC cell growth in tumorigenicity mouse model

To validate the function of ZONs in inhibiting RCC cell growth, we performed tumorigenicity analysis in nude model. As our data shown, the ZONs attenuated the tumor growth in the system and the reduced tumor size, tumor weight, and tumor volume were revealed (Fig. 4A-C). Meanwhile, we identified that miR-27a-3p was enhanced and YAP was reduced in the ZONs-treated group (Fig. 4D and E). Meanwhile, ZONs repressed expression of Twist, and Vimentin and enhanced E-cadherin expression in the model (Fig. 4F).

3.5. ZONs down-regulate YAP expression by inducing miR-27a-3p to suppress RCC cell survival

We found that the expression of miR-27a-3p was enhanced by ZONs in the RCC cells (Fig. 5A). Subsequently, the binding sequence was also identified between miR-27a-3p and YAP and the up-regulation of miR-27a-3p significantly inhibited luciferase activity of YAP mRNA 3′UTR (Fig. 5B and C). The mRNA and protein levels of YAP were reduced by miR-27a-3p in CAKI-1 and 786-O cells (Fig. 5D and E). Meanwhile, ZONs suppressed YAP expression and miR-27a-3p inhibitor reversely affected this result in CAKI-1 and 786-O cells (Fig. 5F). Meanwhile, we validated that the expression of miR-27a-3p was reduced and YAP expression was upregulated in clinical RCC tissues (Fig. 5G). Besides, the expression of f miR-27a-3p was negatively correlated with YAP in clinical RCC tissues (Fig. 5G).

The ferroptosis related phenotypes, such as ROS accumulation and iron/Fe^{2+} levels, were enhanced by miR-27a-3p mimic in CAKI-1, 786-O, and 769P cells (Fig. 5H-K and S4A and B). Meanwhile, the miR-27a-3p mimic repressed expression of Twist, and Vimentin and enhanced E-cadherin expression (Fig. 5L and Fig. S4C).

Furthermore, ZONs reduced viabilities and enhanced apoptosis of CAKI-1, 786-O, and 769P cells, which was reversed by YAP overexpression and miR-27a-3p inhibitor (Fig. 6A and B, and S5A and B). The treatment of ZONs increased the levels of ROS and iron/Fe^{2+} in CAKI-1, 786-O, and 769P cells, while YAP overexpression and miR-27a-3p inhibitor could reverse this effect (Fig. 6C, and S5C). In addition, the expression of SLC7A11 and GPX4 was reduced by ZONs, but YAP overexpression and miR-27a-3p inhibitor rescued the expression in CAKI-1 and 786-O cells (Fig. 6D).

Moreover, we observed that the invasion and migration of CAKI-1 and 786-O cells were repressed by miR-27a-3p, while the overexpression of YAP rescued the phenotype in the cells (Fig. S6A). The miR-27a-3p mimic inhibited expression of Twist, and Vimentin and enhanced E-cadherin expression in CAKI-1 and 786-O cells, in which YAP overexpression reversed the effect in the cells (Fig. S6B). Consistently, the treatment of ZONs suppressed invasion and migration of CAKI-1 and 786-O cells, while YAP overexpression and miR-27a-3p inhibitor rescued the phenotype (Fig. S7A). Besides, the treatment of ZONs reduced expression of Twist,

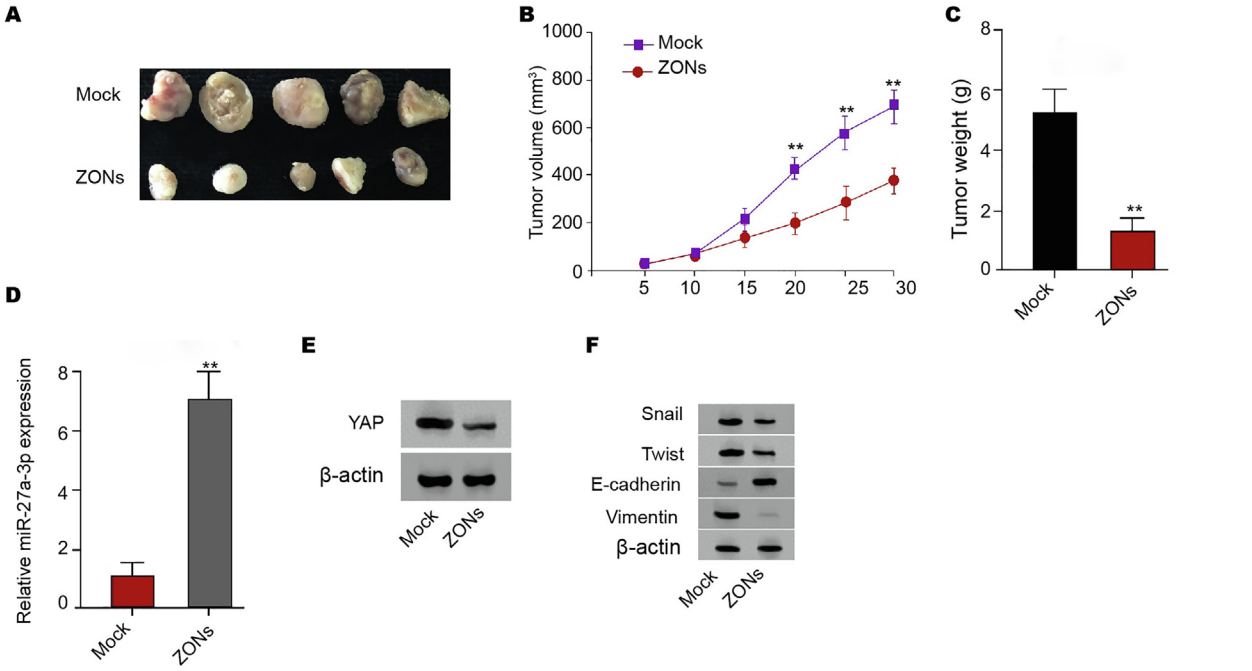

Fig. 4 ZONs suppress RCC cell growth in tumorigenicity mouse model. (A-E) Tumorigenicity analysis of CAKI-1 treated with ZONs. The tumor size (A), tumor volume, (B) and tumor weight (C) were analyzed. The qPCR analysis of miR-27a-3p (D) and Western blot analysis of YAP (E) were conducted in the tumor tissues. (F) The expression of Snail, Twist, Vimentin, and E-cadherin was analyzed by Western blot. N = 5, mean ± SD: ** $P < 0.01$.

and Vimentin and promoted E-cadherin expression in CAKI-1 and 786-O cells, in which YAP overexpression and miR-27a-3p inhibitor could reverse the effect in the cells (Fig. S7B).

4. Discussion

RCC is the prevalent malignancy and is characterized by high mortality and metastasis. Ferroptosis has been identified as an essential process in cancer development, but the regulatory mechanism underlying the RCC progression remains obscure. In the present study, we identified the important role of ZONs in promoting ferroptosis of RCC cells by regulating miR-27a-3p/YAP axis.

It has been found that ferroptosis plays vital roles in RCC progression. The glutathione redox system is critical to regulate ferroptosis related to impaired lipid metabolism in RCC (Miess et al., 2018). Artesunate represses growth of sunitinib-resistant RCC cells by ferroptosis induction and cell cycle arrest (Markowitsch et al., 2020). Meanwhile, Nanoparticles have presented significant therapeutic function in multiple diseases (Abu-Dief et al., 2021). In this study, we found that ZONs induce ferroptosis-like phenotypes in RCC cells. It provides new evidence of the molecular mechanism of ferroptosis in RCC cells. Our data demonstrated that ZONs inhibited cell growth *in vitro* and *in vivo* and repressed invasion and migration of RCC cells. These indicate the new function of ZONs in RCC development.

YAP is a well-known oncogene and affects RCC progression as well. NR1B2 inhibits RCC development by regulating LATS 1/2-YAP signaling (Yin et al., 2019). MiR-10b represses RCC metastasis and invasion by targeting FAK/YAP signaling in RCC (He et al., 2019). Meanwhile, YAP is involved in the regulation of ferroptosis of cancer cells (Sun and Chi, 2021). Intercellular interplay regulates ferroptosis of cancer cells by NF2/YAP signaling (Wu et al., 2019). The Hippo signaling regulator TAZ modulates ferroptosis of renal cell carcinoma cells (Yang et al., 2019). DDR2 contributes to ferroptosis by YAP signaling in recurrent breast cancer (Lin et al., 2021). Meanwhile, the function of YAP in epithelial-mesenchymal transition (EMT) has been reported in multiple cancers, including RCC. For example, it has been reported that EMT transcription factor ZEB1 genome-widely cooperates with YAP in breast cancer (Feldker et al., 2020). The coactivation of Zinc-dependent modulation of ZEB1 and YAP contributes to EMT plasticity and metastasis in pancreatic cancer (Liu et al., 2021). Specifically, NR1B2 inhibits EMT in RCC by regulation of LATS 1/2-YAP signaling (Yin et al., 2019). These studies imply that YAP plays a crucial role in EMT. Meanwhile, it has been reported that miR-27a-3p inhibits metastasis through repressing VE-cadherin expression and suppressing EMT in liver cancer (Zhao et al., 2016). DANCR contributes to liver cancer progression and EMT through targeting miR-27a-3p/ROCK1/LIMK1/COFILIN1 signaling (Guo et al., 2019). Interestingly, miR-27a-3p modulates EMT in oral squamous cell carcinoma cells by targeting YAP (Zeng et al., 2016). These reports imply that miR-27a-3p is involved in the regulation of EMT. However, the effect of miR-27a-3p/YAP axis on EMT in RCC remains unclear. In this study, we identified that miR-27a-3p/YAP axis was involved in ZONs regulated EMT in RCC. It suggests that miR-27a-3p/YAP regulates EMT in RCC and provides the new evidence of the role of miR-27a-3p and YAP in EMT during cancer progression. Targeting miR-27a-3/YAP axis may be a potential therapeutic strategy of RCC treatment. Meanwhile,

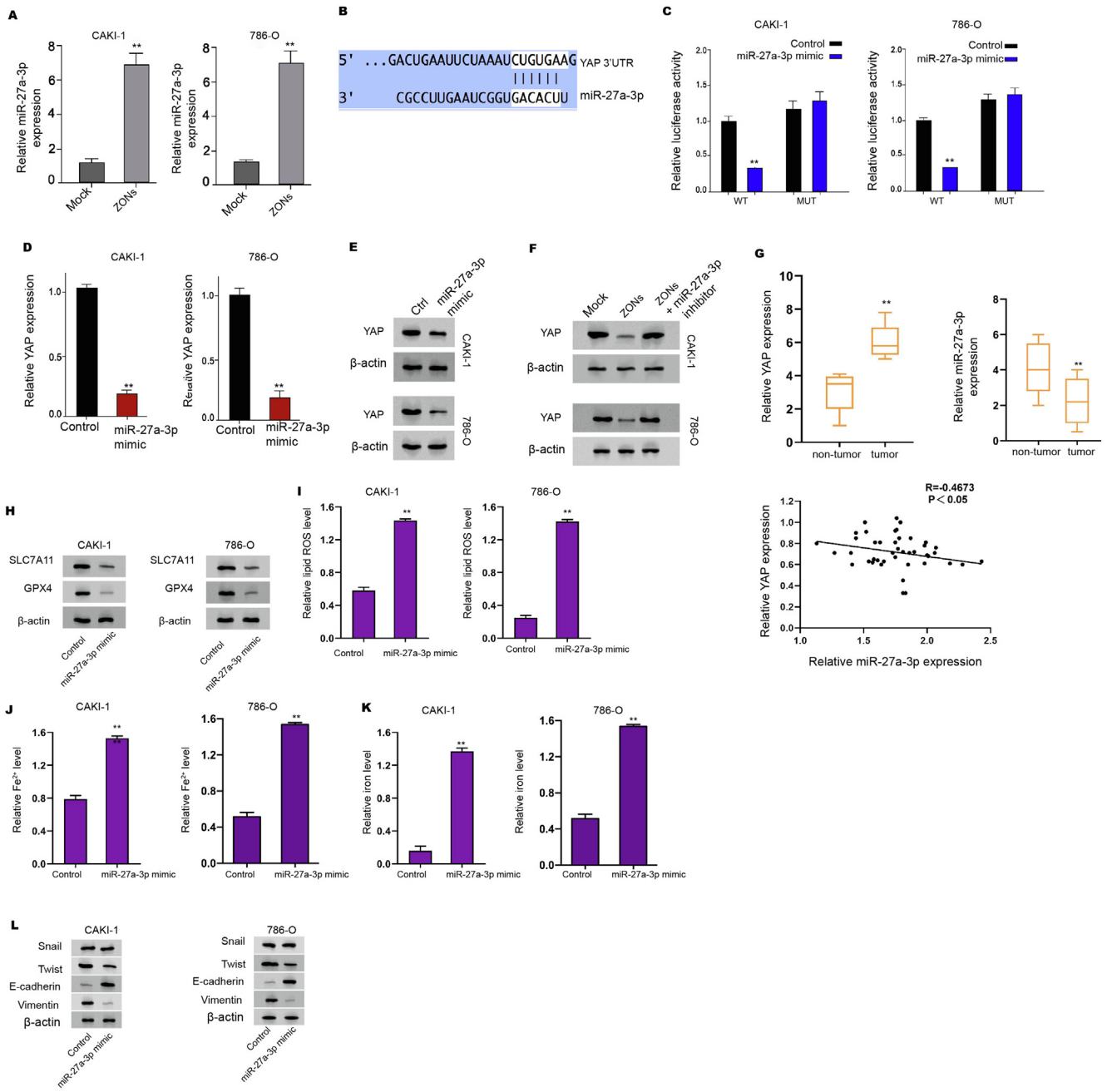

Fig. 5 ZONs up-regulate YAP expression by enhancing miR-27a-3p. (A) The expression of miR-27a-3p was measured by qPCR in the cells treated with ZONs. (B) The binding analysis between YAP and miR-27a-3p in TargetHumanScan database. (C-E) The dual luciferase reporter assays of YAP mRNA 3′UTR (C), the qPCR analysis (D) and Western blot analysis (E) of YAP were conducted in CAKI-1 and 786-Ocells treated with control mimic or miR-27a-3p mimic. (F) The Western blot analysis of YAP was carried out in the CAKI-1 and 786-O cells co-treated with ZONs and miR-27a-3p inhibitor. (G) The expression and correlation of miR-27a-3p and YAP was analyzed by qPCR in clinical RCC tissues (n = 50) and the adjacent non-tumor tissues (n = 50). The Western blot analysis of GPX4 and SLC7A11 (H), ROS analysis (I), iron/Fe^{2+} analysis (J and K) were conducted in the cells treated with miR-27a-3p mimic. (L) The expression of Snail, Twist, Vimentin, and E-cadherin was analyzed by Western blot. N = 3, mean ± SD: ** $P < 0.01$.

we identified that ZONs down-regulated YAP expression by enhancing miR-27a-3p to inhibit RCC cell survival. This data elucidates the downstream mechanism involving miR-27a-3p/YAP axis in RCC development. As the previous reports, YAP is a crucial oncogene to modulate metastasis, apoptosis, and ferroptosis during the cancer development (Wu et al., 2019). These data provide new insight into the mechanism by which ZONs inhibits RCC development by targeting miR-27a-3p/YAP axis.

5. Conclusions

Finally, we concluded that ZONs induced RCC cell ferroptosis to suppress RCC cell survival by targeting miR-27a-3p/YAP

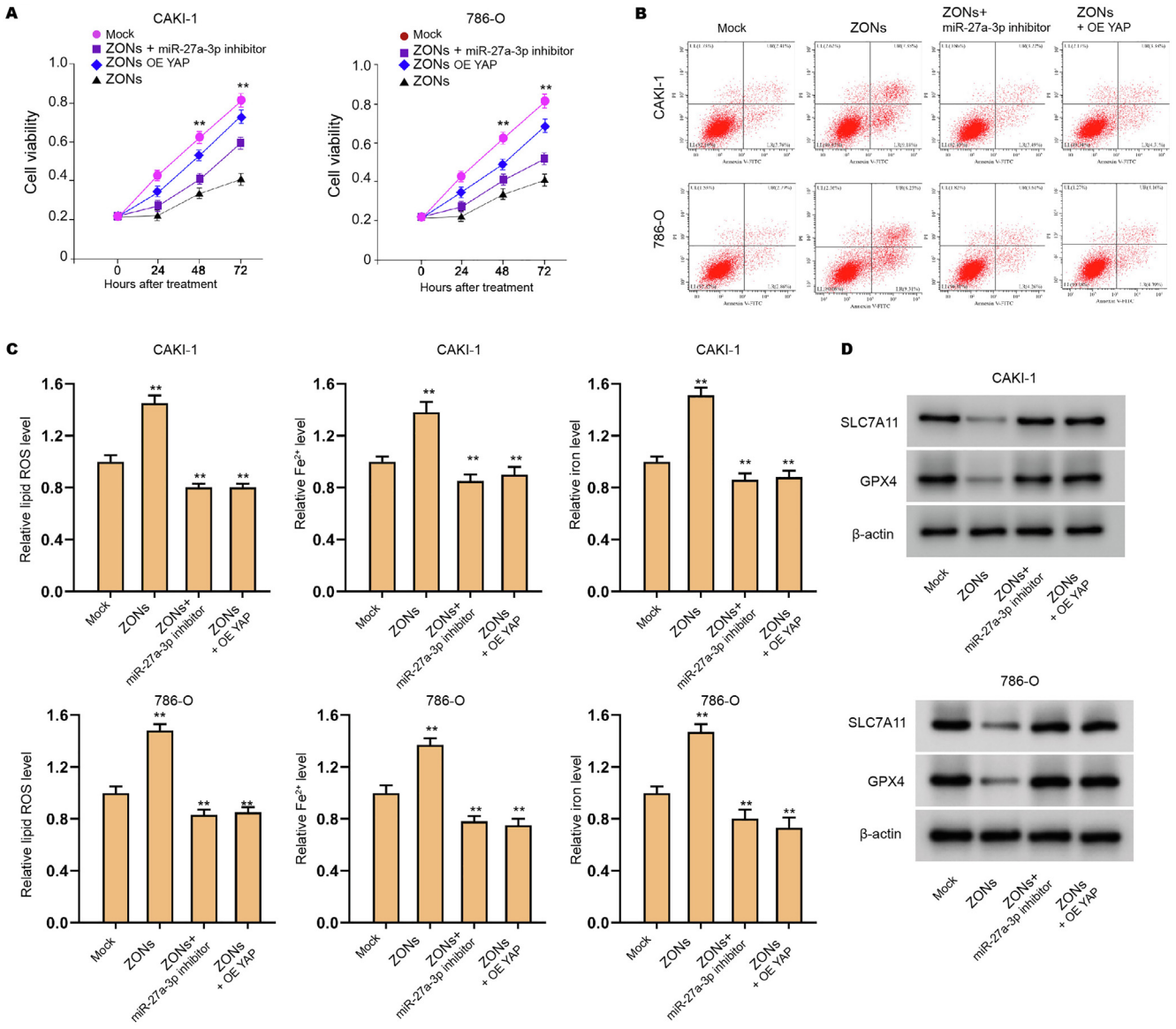

Fig. 6 ZONs down-regulate YAP expression by inducing miR-27a-3p to suppress RCC cell survival. (A-C) The CAKI-1 and 786-O cells were treated with ZONs, or co-treated with miR-27a-3p inhibitor or YAP overexpressing plasmids. The MTT assay (A) and Flow cytometry analysis (B) were carried out. The ROS analysis and iron/Fe^{2+} analysis (C) were conducted. (D) Western blot analysis of GPX4 and SLC7A11. N = 3, mean ± SD: ** $P < 0.01$.

axis. The clinical significance of ZONs for the treatment of RCC is required to further study and may benefit the targeted therapy of RCC.

Declaration of Competing Interest

The authors declare that they have no known competing financial interests or personal relationships that could have appeared to influence the work reported in this paper.

Appendix A. Supplementary data

Supplementary data to this article can be found online at https://doi.org/10.1016/j.arabjc.2022.103753.

References

Linehan, W.M., Ricketts, C.J., 2019. The Cancer Genome Atlas of renal cell carcinoma: findings and clinical implications. Nat Rev Urol. 16, 539–552.

Lucarelli, G., Loizzo, D., Franzin, R., Battaglia, S., Ferro, M., Cantiello, F., et al, 2019. Metabolomic insights into pathophysiological mechanisms and biomarker discovery in clear cell renal cell carcinoma. Expert Rev. Mol. Diagn. 19, 397–407.

Dixon, S.J., Lemberg, K.M., Lamprecht, M.R., Skouta, R., Zaitsev, E. M., Gleason, C.E., et al, 2012. Ferroptosis: an iron-dependent form of nonapoptotic cell death. Cell. 149, 1060–1072.

Miess, H., Dankworth, B., Gouw, A.M., Rosenfeldt, M., Schmitz, W., Jiang, M., et al, 2018. The glutathione redox system is essential to prevent ferroptosis caused by impaired lipid metabolism in clear cell renal cell carcinoma. Oncogene 37, 5435–5450.

Yagoda, N., von Rechenberg, M., Zaganjor, E., Bauer, A.J., Yang, W. S., Fridman, D.J., et al, 2007. RAS-RAF-MEK-dependent oxidative cell death involving voltage-dependent anion channels. Nature 447, 864–868.

Yang, W.H., Ding, C.C., Sun, T., Rupprecht, G., Lin, C.C., Hsu, D., et al, 2019. The Hippo Pathway Effector TAZ Regulates Ferroptosis in Renal Cell Carcinoma. Cell Rep. 28, (2501–8) e4.

Steele, A., Bayer, I., Loth, E., 2009. Inherently superoleophobic nanocomposite coatings by spray atomization. Nano Lett. 9, 501–505.

Hu, C., Du, W., 2020. Zinc oxide nanoparticles (ZnO NPs) combined with cisplatin and gemcitabine inhibits tumor activity of NSCLC cells. Aging (Albany NY) 12, 25767–25777.

Maugeri-Sacca, M., De Maria, R., 2018. The Hippo pathway in normal development and cancer. Pharmacol. Ther. 186, 60–72.

Zeng, G., Xun, W., Wei, K., Yang, Y., Shen, H., 2016. MicroRNA-27a-3p regulates epithelial to mesenchymal transition via targeting YAP1 in oral squamous cell carcinoma cells. Oncol. Rep. 36, 1475–1482.

Wu, J., Minikes, A.M., Gao, M., Bian, H., Li, Y., Stockwell, B.R., et al, 2019. Intercellular interaction dictates cancer cell ferroptosis via NF2-YAP signalling. Nature 572, 402–406.

Markowitsch, S.D., Schupp, P., Lauckner, J., Vakhrusheva, O., Slade, K.S., Mager, R., et al, 2020. Artesunate Inhibits Growth of Sunitinib-Resistant Renal Cell Carcinoma Cells through Cell Cycle Arrest and Induction of Ferroptosis. Cancers (Basel) 12.

Abu-Dief, A., Salaheldeen, M., El-Dabea, T., 2021. Recent advances in development of gold nanoparticles for drug delivery systems.

Yin, L., Li, W., Wang, G., Shi, H., Wang, K., Yang, H., et al, 2019. NR1B2 suppress kidney renal clear cell carcinoma (KIRC) progression by regulation of LATS 1/2-YAP signaling. J. Exp. Clin. Cancer Res. 38, 343.

He, C., Chen, Z.Y., Li, Y., Yang, Z.Q., Zeng, F., Cui, Y., et al, 2019. miR-10b suppresses cell invasion and metastasis through targeting HOXA3 regulated by FAK/YAP signaling pathway in clear-cell renal cell carcinoma. BMC Nephrol. 20, 127.

Sun, T., Chi, J.T., 2021. Regulation of ferroptosis in cancer cells by YAP/TAZ and Hippo pathways: The therapeutic implications. Genes Dis. 8, 241–249.

Lin, C.C., Yang, W.H., Lin, Y.T., Tang, X., Chen, P.H., Ding, C.C., et al, 2021. DDR2 upregulation confers ferroptosis susceptibility of recurrent breast tumors through the Hippo pathway. Oncogene.

Feldker, N., Ferrazzi, F., Schuhwerk, H., Widholz, S.A., Guenther, K., Frisch, I., et al, 2020. Genome-wide cooperation of EMT transcription factor ZEB1 with YAP and AP-1 in breast cancer. EMBO J. 39, e103209.

Liu, M., Zhang, Y., Yang, J., Zhan, H., Zhou, Z., Jiang, Y., et al, 2021. Zinc-Dependent Regulation of ZEB1 and YAP1 Coactivation Promotes Epithelial-Mesenchymal Transition Plasticity and Metastasis in Pancreatic Cancer. Gastroenterology 160, (1771–83) e1.

Zhao, N., Sun, H., Sun, B., Zhu, D., Zhao, X., Wang, Y., et al, 2016. miR-27a-3p suppresses tumor metastasis and VM by down-regulating VE-cadherin expression and inhibiting EMT: an essential role for Twist-1 in HCC. Sci. Rep. 6, 23091.

Guo, D., Li, Y., Chen, Y., Zhang, D., Wang, X., Lu, G., et al, 2019. DANCR promotes HCC progression and regulates EMT by sponging miR-27a-3p via ROCK1/LIMK1/COFILIN1 pathway. Cell Prolif. 52, e12628.